PERGAMON

Pattern Recognition 36 (2003) 2093–2104

PATTERN RECOGNITION
THE JOURNAL OF THE PATTERN RECOGNITION SOCIETY

www.elsevier.com/locate/patcog

Boundary detection of optic disk by a modified ASM method

Huiqi Li[a,*], Opas Chutatape[b]

[a] *Department of Computer Science, School of Computing, National University of Singapore, 3 Science Drive 2, Singapore 117543, Singapore*

[b] *School of Electrical and Electronic Engineering, Nanyang Technological University, Nanyang Avenue, Singapore 639798, Singapore*

Received 10 July 2002; accepted 11 February 2003

Abstract

A new algorithm to automatically detect the boundary of optic disk in color fundus images is proposed. The optic disk is located by principal component analysis (PCA) based model, which is employed to initialize active shape model (ASM) to detect the disk boundary. ASM is modified with two aspects: one is the self-adjusting weight in the transformation from shape space to image space; the other is exclusion of outlying points in obtaining shape parameters. The modifications make the proposed algorithm more robust and converge faster than the original ASM method, especially in the case where the edge of optic disk is weak or occluded by blood vessels.

Keywords: Optic disk; ASM; PCA; Boundary detection; Fundus image

1. Introduction

Color retinal images captured from fundus camera play an important role in the mass screening and diagnosis of eye diseases. Extraction of main structures in retinal images is fundamental and useful for automatic processing of retinal images. Boundary detection of optic disk is elementary among all the structures not only because optic disk acts as landmark and reference to other structures but also because the shape of optic disk itself can be used to assess the progress of eye diseases such as glaucoma. However, it is not a simple task to detect the shape of optic disk accurately and reliably, as some parts of the boundary are not well defined and some parts are obscured by blood vessels.

Model based method has attracted much interest in the application of facial and medical images. Deformable model is widely investigated especially in the segmentation, matching and tracking of medical structures [1]. The deformable model is characterized as a model that deforms the shape to match a known object in a given image. It can be classified into either free-form models or parametric models. For free-form deformable models, there is no global structure of the template except some general regulation constraints. The active contour or 'snakes' model [2] is a typical one. For parametric deformable models, the deformations are controlled by a set of parameters that can determine a specific characteristic shape and its variation. Active shape model (ASM) introduced by Cootes and Taylor [3] belongs to parametric deformable model, which combines point distribution model (PDM) and an iterative refinement procedure. ASM can describe the shape of non-rigid objects, therefore it is efficient in many applications especially in the extraction of anatomical structures. Though a high degree of a priori knowledge is available, the anatomical structures are complex and individually variable.

In one approach, Hough transform was employed to obtain the estimated outer circle of optic disk based on the result of edge detection [4,5]. The edge of optic disk was enhanced to detect edge points before Hough transform was applied. The outer circle of the optic disk was determined by the parameters having the maximum counts. In another approach, optic disk contours were estimated by the Hausdorff-based [6] matching between the detected edges and the template of circle with different sizes in Ref. [7].

* Corresponding author. Tel.: +65-68744889; fax: +65-67791610.

E-mail address: dcslihq@nus.edu.sg (H. Li).

0031-3203/03/$30.00
doi:10.1016/S0031-3203(03)00052-9

These are the simplest top-down strategies which can result in the approximate circle of the optic disk boundary. The obtained circle will not exactly match the optic disk boundary, since the normal optic disks are not round but vertically slightly oval, not to mention the change of its shape due to certain diseases. Snakes was applied to detect the exact contour of optic disk in Refs. [8,9]. The major advantage of the algorithm is its ability to bridge discontinuities in the image feature being located. The boundary detected by Morris and Donnison [8] bulged inwards where optic disk boundary crossed blood vessels. This drawback was later considered by the snake algorithm proposed in Ref. [9], where the stiffness criterion was included and the energy function was minimized differently. However, the algorithm was sensitive to the preprocessing, and the method was not fully automatic as well because a manual initialization was required.

In this paper, a new method of fully automatic extraction of optic disk in color retinal images is proposed. The optic disk is located by principal component analysis (PCA) based model, which is used to initialize ASM automatically. This is the first time that the ASM is applied to the feature extraction in fundus images. It takes advantage of top-down strategy to get robust result. The original ASM is modified in two aspects. Firstly, adjustable weight is applied in the transform between model space and image space instead of fixed weight factors. Secondly, the mismatched points are not used in the projection onto shape space to obtain shape parameters. Such improvement makes the algorithm more favorable for the case of weak edges or noises. The investigated algorithm is not restricted to fundus images but can be applied to other applications involving deformable shapes as well.

2. Locating optic disk by PCA

The optic disk is located by PCA-based model [10], which is described in detail in [11]. The first step is the training procedure to obtain 'disk space'. A square sub-image around optic disk is cropped from each fundus image for training. The sub-images are resized to $L \times L$ pixels and their intensity is rescaled to the same range to form a training set. Each training image can be viewed as a vector of L^2. L is set to 90 in our application, because most of the optic disk diameters are able to fit well into this size though they are in the range of 65–100 pixels. The technique of PCA is employed to the training set to get the modes of variation around the average image. Ten optic disk images are carefully selected as the training set and the first six eigenvectors corresponding to the largest six eigenvalues are chosen to represent the training set. The subspace defined by the eigenvectors is termed as disk space. The model obtained by PCA statistical analysis is put to use in the localization of optic disk in new fundus images.

For each test image, the pixels with the highest 1% gray levels in intensity image are selected, as optic disk occupies 1–3% of the whole retinal image. The selected pixels are clustered by the Single Pass method [12]. The clusters having centroids within a specified distance are combined. For each cluster having more than 100 pixels after combination, an optic disk candidate region is defined as a square of 120×120 pixels with the centroid of the cluster as its center. At each pixel in the candidate regions, a sub-image of $L \times L$ pixels (scale $= 1$) with the pixel as the center is obtained automatically. The Euclidean distance between the corresponding pixels of the sub-image and its reconstruction from disk space is calculated to locate optic disk. Different scales (0.8–1.1) are applied in order to detect the optic disk of different sizes. The pixel (L_x, L_y) with the minimum distance among all the scales is located as the center of optic disk, as the distance indicates the similarity of optic disk.

3. Deriving PDM

PDM, which was first proposed by Cootes and Taylor [3], is a method for building model by learning patterns of variability from a training set of correctly annotated shapes. The model allows deformation in certain ways that are consistent with the training set. The PDM can thus be used to locate new instance of such shapes in other images.

A shape in a 2-D image can be described by the position of a set of n landmark points which can also be represented as a point in the $2n$-D landmark space. The landmark points are manually annotated on the edge of main blood vessels inside optic disk or on the disk boundary in a set of training images. m training shapes will form a distribution of m points in the $2n$-D space. PCA of the distribution is carried out to derive a statistical description of the shape and its variations as shown in the following. The model thus obtained is called PDM.

The training shapes need to be aligned into a common coordinates before PCA transform. The aligning of shapes is aimed to minimize the sum of squared distances between the landmark points on different shapes. Denoting two shapes in the training set as x^1 and x^2, each shape can be described as a vector of n coordinate pairs

$$x^1 = (x_1^1, y_1^1, x_2^1, y_2^1, \ldots, x_n^1, y_n^1)^{\mathrm{T}},$$
$$x^2 = (x_1^2, y_1^2, x_2^2, y_2^2, \ldots, x_n^2, y_n^2)^{\mathrm{T}}, \quad (1)$$

where (x_i^j, y_i^j) is the position of the ith point on the shape $x^j, j = 1, 2$. The center of the gravity is already translated to origin in x^1 and x^2. The aligning of the two shapes is done by the transform Γ applied to x^2, which composes of translation (t_x, t_y), rotation θ, and scaling s:

$$\Gamma(x^2) = \begin{pmatrix} s\cos\theta & -s\sin\theta \\ s\sin\theta & s\cos\theta \end{pmatrix} \begin{pmatrix} x_i^2 \\ y_i^2 \end{pmatrix} + \begin{pmatrix} t_x \\ t_y \end{pmatrix}. \quad (2)$$

The best parameter vector $\tau(s, \theta, t_x, t_y)$ of the transformation Γ to align shape x^2 and x^1 can be selected by minimizing the following expression (3) using a routine least-squares approach, i.e., the parameter τ is obtained by $\partial E_\tau / \partial \tau = 0$:

$$E_\tau = (x^1 - \Gamma(x^2))^{\mathrm{T}}(x^1 - \Gamma(x^2)). \tag{3}$$

PCA is then performed on the aligned training shapes. A shape can be approximated by

$$x = \bar{x} + \Phi b, \tag{4}$$

where $\bar{x}$ is the mean shape of the aligned training set, $b = (b_1, b_2, \ldots, b_t)^{\mathrm{T}}$ is a vector of shape parameters, $\Phi = (\Phi_1, \Phi_2, \ldots, \Phi_t) \in R^{2n \times t}$ is the set of eigenvectors corresponding to the largest t eigenvalues of the covariance matrix S. Denoting the training shape after alignment as $\hat{x}^i = \Gamma(x^i) = (\hat{x}^i_1, \hat{y}^i_1, \hat{x}^i_2, \hat{y}^i_2, \ldots, \hat{x}^i_n, \hat{y}^i_n)^{\mathrm{T}}$,

$$S = \frac{1}{m-1} \sum_{i=1}^{m} (\hat{x}^i - \bar{x})(\hat{x}^i - \bar{x})^{\mathrm{T}}. \tag{5}$$

The eigenvalue of S is equal to the variance of the shapes described by the corresponding eigenvector. The eigenvectors provide the mode of variation, a way in which the landmark points move together as the shape varies. PDM is derived by formula (4), which is a statistical description of the shape and its variation of the training set. The space defined by formula (4) is referred to as shape space. In the application of optic disk boundary detection, a shape instance is represented by the positions of 48 points, i.e., $n = 48$. This is a proper number to describe the boundary according to our tests and observation. Fig. 1 shows an example of the landmarks in one training image and its corresponding shape instance. Fourteen points (point 1–8, 25–30) are selected on the main blood vessels inside optic disk to constrain the representation of the shape model of optic disk. The other points (9–24 and 31–48) are chosen evenly on the boundary of the optic disk. Eight shapes of optic disk are employed here to train the PDM, i.e., $m = 8$. The model obtained for the left eye and the effect of varying each of the first four model parameters in turn between ± 3 standard deviations are presented in Fig. 2. The variance of the shapes in the training set can be approximately described by the first t modes, where t is chosen as four in this application. These first four modes represent 93% of the total variance of shapes in the training set which can be verified from

$$k = \frac{\sum_{i=1}^{t} \lambda_i}{\sum_{i=1}^{m} \lambda_i} \times 100\%, \tag{6}$$

where k represents the proportion of the total variation, λ_i is the ith largest eigenvalue of covariance matrix S. A new shape can be generated by formula (4) with the proper shape parameter vector b. The advantage of the PDM is its ability to learn the characteristic pattern of a shape class and its ability to deform in a way that reflects the variation in the training set.

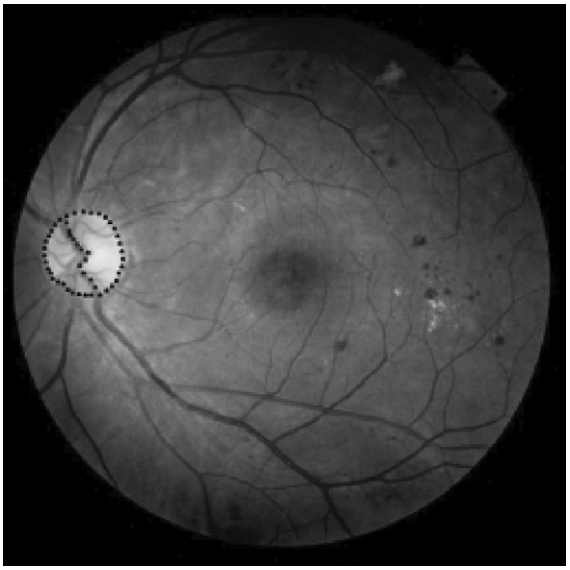

(a)

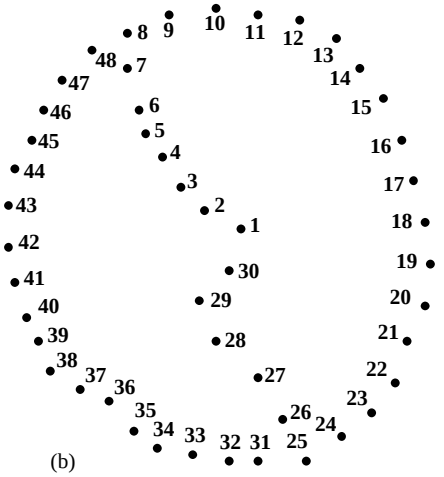

(b)

Fundus image No.14

Fig. 1. Landmarks of the optic disk on the fundus image of a left eye. (a) A fundus image with annotation of 48 landmark points. (b) The corresponding shape instance.

4. ASM and a modified ASM

4.1. ASM

ASM method is an iterative searching procedure to fit the PDM in a new image to find the modeled objects. The algorithm is termed as 'active shape model' because the model deforms to fit the data better, but only in the ways

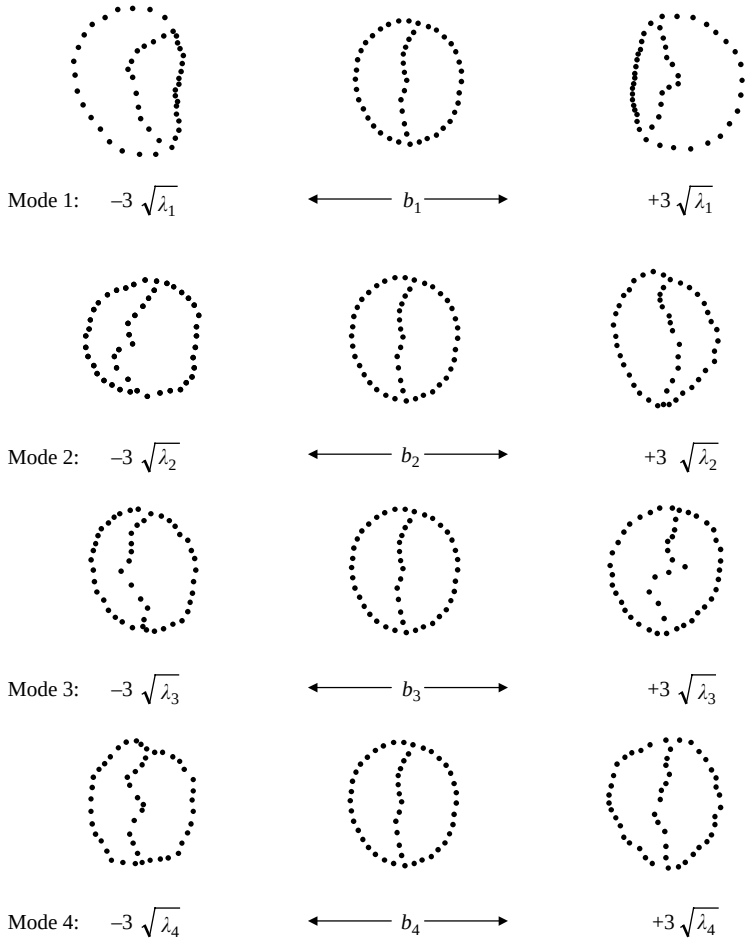

Fig. 2. The first four modes of variation from −3 to +3 standard deviation, the middle column shows the mean shape of the aligned training set.

that are consistent with the shapes in the training set [3]. The procedure includes the following five steps:

4.1.1. Initialization

The space defined by the input image is referred to as image space, compared with shape space described by formula (4). The shape model in the shape space is denoted by the lowercase and shape instance in the image space is represented by uppercase in this paper. The transform defined in formula (2) can also be used to transform the shape model from shape space to image space. The model instance in image space is initialized by choosing proper pose parameter vector $\tau(s, \theta, t_x, t_y)$ and shape parameter vector b. The mean shape of the PDM derived in formula (4) is employed as the primitive shape model in shape space, i.e. $b_i = 0, i = 1 \sim t$. The initialization of ASM is performed automatically in a new image according to the localization of the optic disk (L_x, L_y) obtained in Section 2, where $s = 1,\ \theta = 0,\ t_x = L_x, t_y = L_y$.

4.1.2. Matching point detection

To each landmark point on the model in the image space, the best matching point is searched, to where the landmark point will be moved. The profile normal to the model boundary is searched while the profile tangent to the boundary is also considered to find the matching points in the application of boundary estimation of optic disk. Fourteen points (point 1–8, 25–30) in the model should be matched to the edge of blood vessels inside optic disk and the other points (9–24 and 31–48) should be fitted to the boundary of the optic disk according to the criterion for selecting the landmark points.

The intensity distribution of a blood vessel's cross-sectional profile can be modeled as a negative step gate function or Gaussian function, while the intensity distribution along the profile normal to the disk boundary can be simplified as a positive or negative step function. The profile in the direction from the center to outside of optic disk is calculated since the location of optic disk center is known approximately. Thus, the profile of the edge can

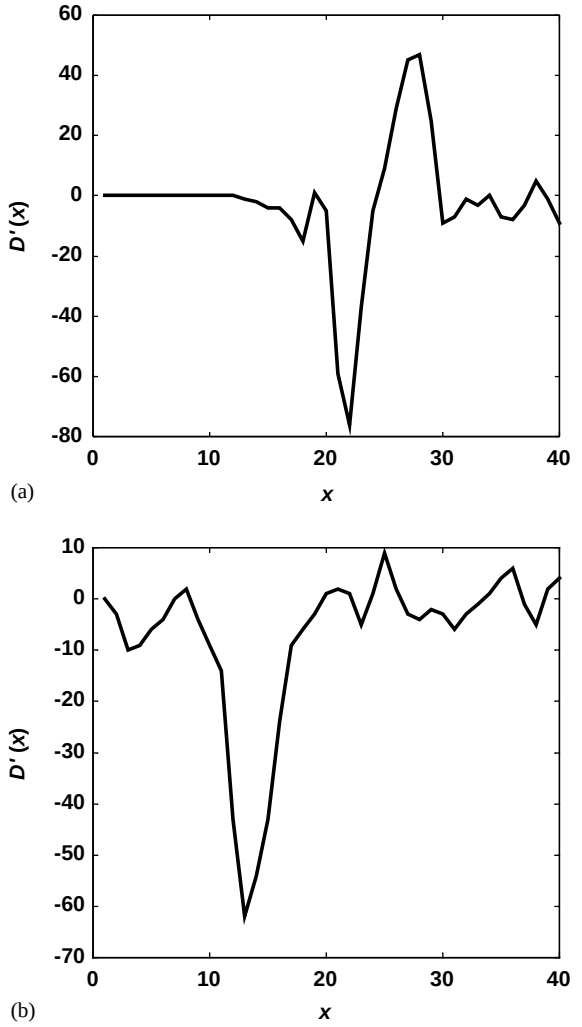

Fig. 3. Practical first derivatives of intensity distribution across blood vessel (a) and the edge of optic disk (b).

be modeled only by the negative step function and not the positive step function. The first derivative $D'(x)$ of the function could be used to distinguish between blood vessel and disk edge. The first derivative $D'(x)$ of a pixel is approximated by the intensity difference of the two pixels adjacent to it along the profile in the practical image. Fig. 3 shows the first derivative $D'(x)$ of intensity distribution across blood vessels and across the boundary of optic disk in a typical fundus image. The presence of blood vessel is identified by a negative pulse followed by a positive pulse within the width range of blood vessels as compared with a single negative pulse where disk edge appears.

Some blood vessels inside the optic disk run in the similar direction to the normal of the model boundary, so the first derivative of the intensity distribution profiles along the normal and tangent to the model boundary are both employed to avoid matching the points wrongly between the edge of optic disk and blood vessels. For landmark points 1–7 and 26–30 (refer to Fig. 1), the point on the strongest edge or nearest edge of blood vessel along the normal profile through the landmark point is identified as the matching point. For the landmark points 8 and 25, the strongest edge on the normal profile belonging to the blood vessel's edge on its tangent profile is detected as the matching point. For landmark points 9–24 and 31–48, the strongest edge on the normal profile that does not belong to blood vessel on the tangent profile is determined as the matching point. The matching points that cannot be searched successfully are estimated from the nearby matching points. The original landmark points will be used as the matching points for those which cannot be estimated by the nearby matching points when their nearby matching points are also not available.

4.1.3. Transformation

Find the pose parameter vector $\tau(s,\theta,t_x,t_y)$ that maps the shape model in shape space to the new matching points in image space by the transform Γ defined by formula (2). The parameter $\tau(s,\theta,t_x,t_y)$ of the transform Γ can be obtained by minimizing the following expression:

$$E_\tau = (Y - \Gamma(x))^{\mathrm{T}}(Y - \Gamma(x)), \tag{7}$$

where Y is the set of matching points in image space, x is the shape model in shape space.

4.1.4. Model update

The inverse of the transformation obtained in Section 4.1.3 is used to transform the matching points Y back to y in the shape space. The shape parameter vector b is updated by projecting the transformed matching points y onto the shape space

$$b = \Phi^{\mathrm{T}}(y - \bar{x}), \tag{8}$$

where y is the transformed matching points to shape space, Φ and $\bar{x}$ are the same definitions as in formula (4). The constriction to b is applied by

$$|b_i| \leqslant 3\sqrt{\lambda_i}, \quad i = 1 \sim 4. \tag{9}$$

This is selected as a suitable limit to b_i since most of the population lies within three standard deviations of the mean [3]. Thereafter a new shape model can be generated by substituting the shape parameter vector b into formula (4).

4.1.5. Convergence evaluation of the shape model

Denoting the derived shape model of the nth iteration and $(n-1)$th iteration in the image space as X^n and X^{n-1}, respectively, the convergence is evaluated according to the following formula:

$$E_X = \|X^n - X^{n-1}\| < \varepsilon_T \quad \text{for a small constant } \varepsilon_T, \tag{10}$$

where E_X is the Euclidean distance between X^n and X^{n-1}. As E_X oscillates sometimes, the shape model is thought to be converged if condition (10) is satisfied in the last five

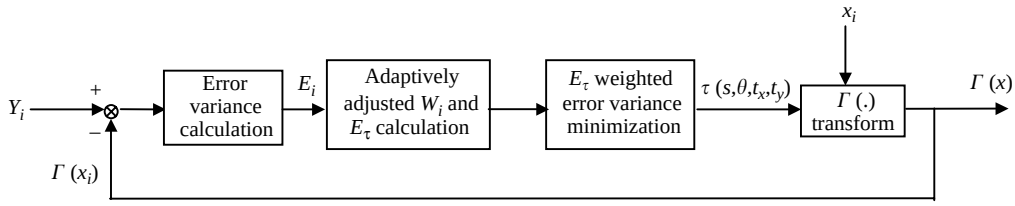

Fig. 4. Diagram of the adjustment of W_i.

iterations. The iteration stops when the shape model is converged and at the same time there are less than 10 landmark points in the shape model whose matching points cannot be detected directly. This is to guarantee the obtained model fits the practical disk edge well. Otherwise the algorithm is iterated from Section 4.1.2 until a preset number is reached.

4.2. A modified ASM

Though ASM is quite robust in detecting the modeled shape, the resultant shape is not satisfactory in some cases. Some matching points may be misplaced in the detection due to weak edges or noises, which make the obtained shape not properly fit the boundary in the image. Two aspects are proposed in this paper to improve the original ASM algorithm.

4.2.1. Self-adjusting weight transform

The proposed transform Γ from the shape space to the image space is defined in the same way as formula (2). Parameter vector $\tau(s,\theta,t_x,t_y)$ is selected to minimize a weighted sum of squares measure of point difference, which can be obtained by $\partial E_\tau/\partial\tau = 0$, where E_τ, being different from Eq. (3), is defined as follows:

$$E_\tau = \sum_{i=1}^{n} (Y_i - X_i)^{\mathrm{T}} W_i (Y_i - X_i)$$

$$= \sum_{i=1}^{n} (Y_i - \Gamma(x_i))^{\mathrm{T}} W_i (Y_i - \Gamma(x_i)), \tag{11}$$

where Y_i and X_i are the positions of ith point of the matching points and the shape model in the image space, respectively. Also x_i is the shape model in the shape space, and W_i is the weight factor.

For each iteration, the transform Γ is performed twice: once for the initialized weight factor W_i and once for the adjusted W_i. Weight factor W_i is initialized to different values according to how its corresponding matching point Y_i is obtained in that iteration. As described in Section 4.1.2, the matching point is either estimated from nearby matching points or set to the landmark point when direct detection is not successful. Largest W_i will be set to those having their matching points detected directly; Smaller W_i will be assigned to the points having their matching points estimated from the nearby matching points; For those having their matching points updated by the original landmarks, the corresponding weight W_i is set to zero to eliminate their effect in the transformation. In our application, W_i is initialized as

$$W_i = \begin{cases} 1 & Y_i \text{ can be detected,} \\ 0.7 & Y_i \text{ can be estimated by} \\ & \quad \text{nearby matching points,} \\ 0 & Y_i \text{ is updated by } X_i. \end{cases} \tag{12}$$

The pose parameter vector τ is calculated and the shape model is transformed to the image space by the parameter vector τ, which is the first transformation in the iteration. In the second transformation, the weight factor W_i for which matching point can be detected or estimated in the iteration is adjusted according to E_i, which is Euclidean distance between the matching point Y_i and the corresponding transformed shape model X_i in the image space presented in

$$E_i = (Y_i - X_i)^{\mathrm{T}}(Y_i - X_i)$$

$$= (Y_i - \Gamma(x_i))^{\mathrm{T}}(Y_i - \Gamma(x_i)), \tag{13}$$

where $Y_i, x_i \in R^{2\times 1}$, $i = 1,2,\ldots,n$. W_i is set to be piece-wise reciprocal ratio of the Euclidean distance E_i. In the application of boundary estimation of optic disk, W_i is adjusted from formula (14). It can be set to other proper values in other applications

$$W_i = \begin{cases} 1, & E_i < 5, \\ 5/E_i, & 5 \leqslant E_i \leqslant 15, \\ 1/E_i, & E_i > 15. \end{cases} \tag{14}$$

The adjustment process of W_i can be depicted as a closed loop block diagram in Fig. 4. The pose parameter vector $\tau(s,\theta,t_x,t_y)$ is updated by minimizing formula (11) with the adjusted W_i described in formula (14). The shape model in the shape space is transformed to the image space again by applying the newly obtained pose parameter vector $\tau(s,\theta,t_x,t_y)$.

With the procedure as described above, the initialization and adjustment of weight factor W_i is not fixed or kept the same in each iteration. The effect of the pose parameter obtained using the initialized W_i is employed to adjust W_i. Thus the concept of feedback is used, for which it is called self-adjusting weight transform. By this improvement, the

misplaced matching points will not affect the transform as much as the correct matching points so that a better parameter vector τ is obtained to align the shape model to the matching points in image space.

4.2.2. Exclusion of outlying points in obtaining shape parameter vector b

The mismatched points not only affect the pose parameters but also the shape parameter vector b when projecting the transformed matching points onto the shape space. If the obtained shape instance is compared with the matching points set, they may not fit very well because of the constraint of the shape parameter vector b and the influence of the misplaced matching points. When the Euclidean distance E_i between the matching point and the corresponding point on the shape model updated by the original ASM method is larger than a certain value, the matching point is considered to be an outlying point or a misplaced matching point. Those outlying points will not be used in the procedure of obtaining shape parameter vector b. In other words, the dimension of landmark space is decreased from $2n$ to $2(n-n_m)$, where n_m is the number of misplaced matching points in the iteration. The shape parameter vector b is therefore determined only by the matching points that fit the boundary well

$$b = \tilde{\Phi}^{\mathrm{T}}(\tilde{y} - \tilde{\bar{x}}), \tag{15}$$

where $b \in R^t$, $\tilde{\Phi} \in R^{2(n-n_m)\times t}$, $\tilde{y} \in R^{2(n-n_m)}$, $\tilde{\bar{x}} \in R^{2(n-n_m)}$. $\tilde{y}$ is the matching points set in the shape space after the outlying points are excluded. $\tilde{\Phi}, \tilde{\bar{x}}$ are the eigenvectors and mean shape in the $2(n-n_m)$ dimensional space corresponding to Φ and $\bar{x}$ in formula (4).

The final shape is estimated as in formula (4) by reconstructing the shape instance in $2n-D$ landmark space with the same parameter vector b obtained from formula (15), by which the achieved shape model will match the boundary of optic disk better than the original ASM especially in the case that more than one matching points are misplaced.

5. Evaluation

The accuracy of an obtained shape instance is evaluated by comparison with a reference shape. The reference shape is annotated manually under the supervision of ophthalmologists. Mean corresponding distance is employed here to assess the accuracy. Distance to the closest point (DCP) for a point a_i on shape A to shape B [13,14] is defined by

$$DCP(a_i, B) = \underset{j=1}{\overset{n}{\mathrm{MIN}}} \|b_j - a_i\|. \tag{16}$$

The mean absolute distance (MAD) between the two shapes [14] is derived by

$$MAD(A,B) = \frac{1}{2}\left(\frac{1}{n}\sum_{i=1}^{n} DCP(a_i,B) + \frac{1}{n}\sum_{i=1}^{n} DCP(b_i,A)\right). \tag{17}$$

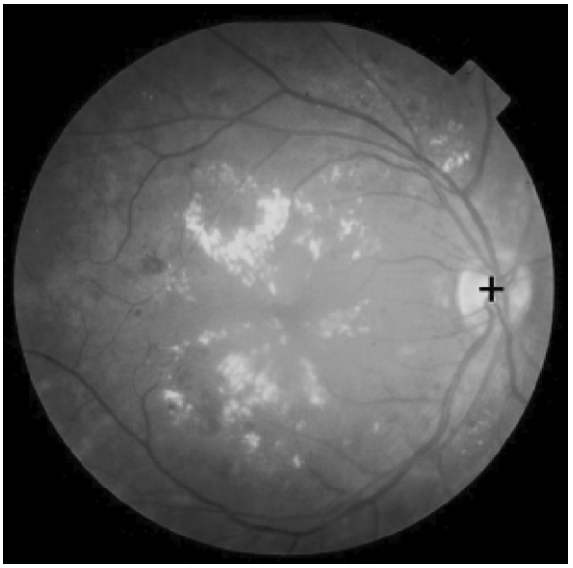

Fundus image No.35

Fig. 5. Optic disk is located by PCA based model, where '+' indicates localization of the center of optic disk.

MAD is a semi-metric, as it does not fulfill the metric condition for triangle inequality. In the application of optic disk boundary detection, positions of landmark points 8–25 and 31–48 in both the reference shape and the obtained shape instance are used to calculate MAD, which evaluates the performance of the applied algorithm.

6. Results and discussion

Thirty-five 24 bits color fundus images of 512 ×512 pixels are tested by the proposed algorithm. These images are all we obtained from clinics, which were captured by a Topcon retinal camera. Six of them are normal fundus images and the other 29 are fundus images with lesions. The proposed algorithm is applied to fundus images of both right eyes and left eyes. The PCA-based model used in locating the optic disk and the PDM in the boundary detection for the right eyes are horizontal mirror images of those for the left eyes.

The center of optic disk to be used for initializing ASM method is located by PCA based model. All the optic disks can be located successfully in the tested 35 images. One of the localization results is illustrated in Fig. 5. It can be seen that the center of the optic disk is identified successfully even in the presence of bright lesions whose area is larger than that of optic disk. In such case, it is usually detected wrongly by bottom-up image processing strategy. The correct localization of optic disk is important for initialization of shape model at a good starting point in ASM, because the ASM algorithm only searches for the matching points

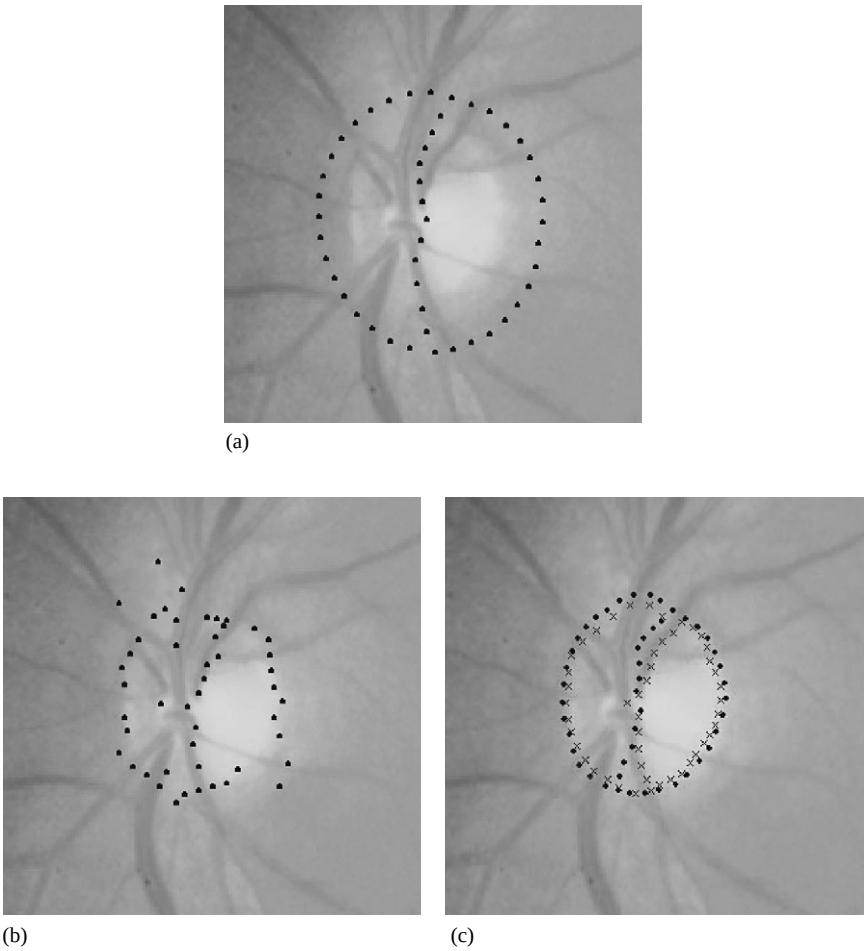

Fig. 6. Example of ASM method. (a) Initialization of the shape model in image space. (b) The matching points. (c) '.'-shape model obtained ($MAD = 2.6771$ pixels), 'x'-reference shape.

around the current position. The shape model will diverge to infinity or converge to an incorrect place with a bad initialization.

ASM comprises initialization of PDM and iterative searching to fit the model to a retinal image. Fig. 6 shows an example of initialization and the achieved shape instance by ASM method. Only the sub-image around optic disk is presented in the figure in order to show the model clearly. In this example, shape model is successfully acquired by ASM method though a couple of matching points does not match the edge of optic disk. By modifying the pose parameter vector τ and shape parameter vector b rather than the model points directly, the shape model is restricted and will not deviate too much from the shape model attained from the training shapes. Here it is shown that ASM method has advantage of top-down strategy and is not sensitive to noises.

The original ASM method could not get satisfactory boundary when the edge of optic disk is weak and occluded by vessels. A modified ASM is proposed to eliminate the influence of the misplaced matching points on transform and in obtaining shape parameter vector b. One example can be seen in Fig. 7. It can be noted in Fig. 7(c) that the boundary at the upper part cannot be detected correctly by ASM. Since the edge at that part is weak, several matching points are located incorrectly such that they affect the final result. Satisfactory result can be obtained by the modified ASM, which is illustrated in Fig. 7(d). In the modified ASM, the transform from model space to image space and the procedure of obtaining shape parameter vector b are both carried out twice. The first round is to identify those misplaced matching points and the second round is to weaken their effect in the transform and exclude them in the projection to model space. The concept of feedback is employed here. Better pose parameter vector $\tau(s, \theta, t_x, t_y)$ and shape parameter vector b are obtained and the result fits the boundary in the image better. Another example is illustrated in

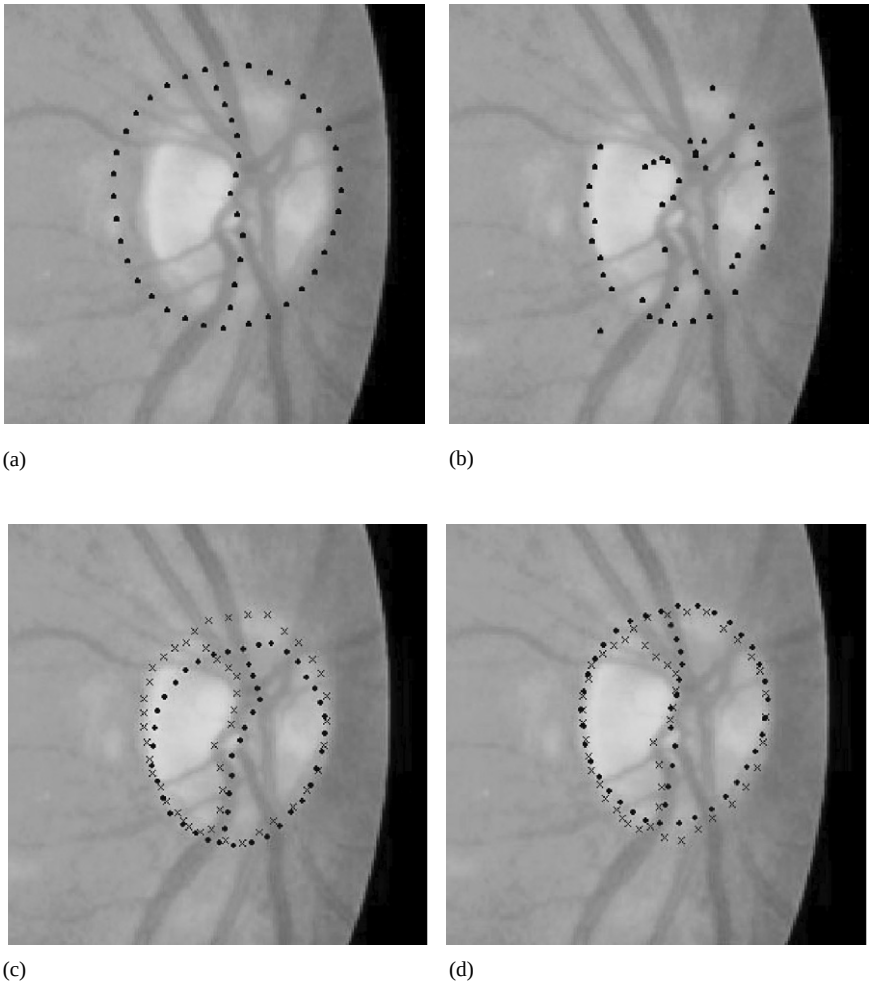

Fig. 7. The modified ASM compared with ASM. (a) Initialization. (b) Matching points obtained by ASM. (c) Shape model obtained by ASM ($MAD = 5.0193$ pixels, 305 iterations). (d) Shape model obtained by the modified ASM ($MAD = 3.6984$ pixels, 12 iterations). 'x' in (c) and (d) indicates the reference shape.

Fig. 8. The shape model could not converge even after 1000 iterations and showed the tendency to converge to the wrong place. The modified ASM could obtain a more suitable result in the same image and required only 33 iterations.

The comparison result of the modified ASM with the original ASM is presented in Table 1. Among the 35 images, the first eight images in the table are employed as the training set to derive PDM. The modified ASM detects the boundary of optic disk successfully in 33 of the images. The original ASM fails in seven of them where G (Great improvement) is marked in the table to indicate that the modified ASM gains much better results than the original ASM. In the other 26 images, the modified ASM also achieves better than or at least as good as the results of ASM. The modified ASM needs less iterations in all the images except two cases (image Nos. 15 and 32). The edges of the optic disk in these two cases are very weak such that there are more than ten points in the shape model that their matching points cannot be detected directly. The boundary detection results by the modified ASM are nevertheless better than ASM in these two images as indicated by the MAD value. Fig. 9 illustrates the convergence of E_X by ASM and the modified ASM in image No.24 where both methods obtain satisfactory results. It can be seen that the modified ASM converges much faster than the original ASM. All these tests show that the modified ASM is more robust and time efficient. Both of the modified ASM and the original ASM failed in two cases (image Nos. 12 and 16), where a large part of the disk edge cannot be identified even by human eyes. A large area of lesion presents near the optic disk in one case (image No.12) and in another case (image No.16) the blood vessels obscure most part of the edge of optic disk. The manual outlining

Table 1
The performance comparison between the modified ASM and ASM

Image no.	Iterations ASM	Iterations Modified ASM	MAD ASM	MAD Modified ASM	Results
1	18	16	5.0448	4.3641	S
4	48	14	4.6473	2.2862	S
14	828	15	5.6567	2.5938	S
18	35	6	3.6437	2.2859	S
23	17	6	2.3275	2.2757	S
31	22	6	3.1453	2.7814	S
32	797	1000	4.2982	3.7551	S
35	305	12	5.0193	3.6984	S
2	46	18	3.1265	2.2987	S
3	245	7	2.6771	2.1603	S
5	84	6	2.2409	3.7083	S
6	399	9	4.5827	2.8439	S
7	67	8	4.7695	2.6716	S
8	14	8	4.0350	2.8698	S
9	71	8	3.7133	3.9858	S
10	1000	8	8.4531	3.1544	S/G
11	15	9	2.8921	2.9592	S
12	66	54	21.4686	14.7338	F (1)
13	51	6	3.3051	2.5307	S
15	247	1000	3.6638	2.8408	S
16	1000	468	61.6681	35.6483	F (2)
17	18	6	4.3589	3.2120	S
19	9	7	3.1432	2.0288	S
20	11	7	7.7570	3.9748	S/G
21	1000	33	13.9465	3.1769	S/G
22	55	24	13.3337	2.9144	S/G
24	88	6	3.6359	2.7279	S
25	317	8	7.3253	3.5710	S/G
26	600	12	5.3209	2.9303	S
27	33	16	3.3229	3.2292	S
28	182	25	5.4281	2.9681	S
29	671	28	7.8496	5.3080	S/G
30	63	13	3.6428	3.1416	S
33	15	6	4.1671	2.8198	S
34	747	11	44.7091	1.8876	S/G

F: fail; S: success; G: great improvement; MAD: mean absolute distance. (1) A large part of disk edge could not be identified even by human eyes due to large area of lesions. (2) Blood vessels obscure most part of the edge of optic disk.

of the blur part of disk edge in these two images was performed according to experience and its symmetric part of edge. The modified ASM obtains better result than the original ASM in both of these two cases. More constraints such as the size of the optic disk could be further investigated to improve the performance of the algorithm.

7. Conclusion

A new and robust algorithm is proposed in this paper to detect the boundary of optic disk automatically. The PCA based model is implemented for the localization of the optic disk for the first time, which enables the automatic initialization of ASM. PDM is obtained from the training set and it is used to search the best fit to a fundus image in ASM algorithm. The modified ASM is later proposed to eliminate the influence of the misplaced matching points in the transform and in obtaining shape parameters. The result is compared with the original ASM method, which shows that the modified ASM is more robust and converges faster than the original ASM. The improvement makes the algorithm more favorable for the cases of weak edges and in the presence of noises where several matching points are misplaced. More images will be tested when more clinical data are available. The achieved result is useful for the further investigation of automatic understanding of fundus images and will facilitate the clinical diagnosis. It is certain that the proposed algorithm will not be limited only to fundus images but it should be applicable to other images as well.

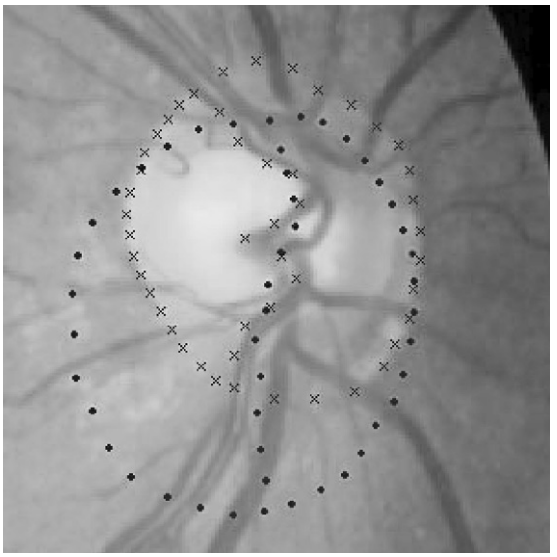

(a)

(b)

Fundus image No.21

Fig. 8. The modified ASM can obtain more robust result than ASM method. '.'-obtained shape; 'x'-reference shape. (a) Result of ASM ($MAD = 13.9465$ pixels, 1000 iterations). (b) Result of the modified ASM ($MAD = 3.1769$ pixels, 33 iterations).

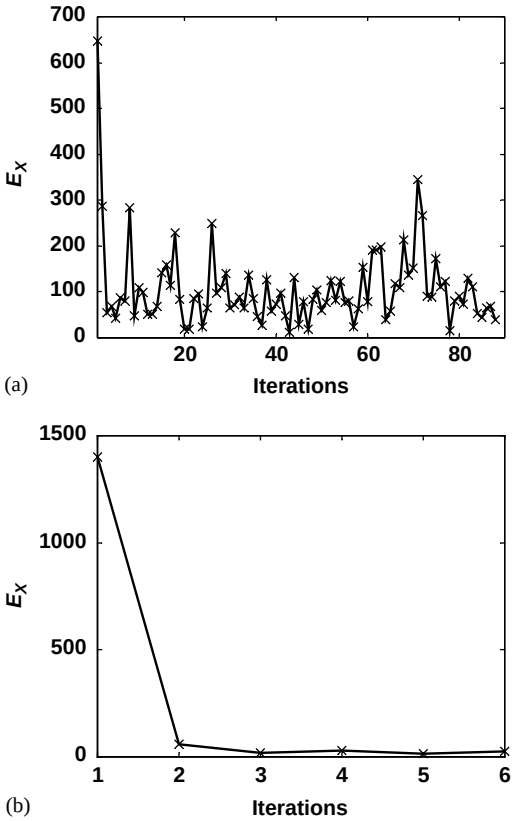

Fig. 9. The convergence of the shape model. (a) Example of E_x by ASM. (b) Example of E_x by the modified ASM.

8. Summary

A new algorithm to detect the boundary of optic disk automatically in color fundus images is proposed in this paper. The optic disk is located by PCA based model. The pixel with the minimum distance in the candidate regions among all the scales is located as the center of optic disk. Once its location is known, the PDM for the estimated shape of optic disk is initialized for further application of the ASM. This is the first time that the ASM is applied to the feature extraction in fundus images. In the matching point detection, the first derivative of the intensity along the normal and tangent profile of the model boundary is used to distinguish between blood vessel and disk edge. The original ASM is modified with two enhanced aspects: one is the self-adjusting weight factor in the transformation from shape space to image space; the other is exclusion of outlying points in the obtaining of shape parameters. In the modified ASM, the transform from model space to image space and the procedure of obtaining shape parameter vector are both carried out twice. The concept of feedback is employed here to avoid the influence of the misplaced matching points. Thirty-five color fundus images obtained from clinics were tested by both the original ASM and the modified ASM. The accuracy is evaluated by the MAD between the obtained shape instance and the reference shape. The test shows that the proposed modifications not only make the algorithm converge faster but also make it more robust than the original ASM method. The improvement makes the algorithm more

favorable for the cases of weak edges and in the presence of noises where several matching points are misplaced. More images will be tested when more clinical data are available. The results obtained can offer further improvement to the automatic processing and understanding of fundus images. The proposed algorithm should also be applicable to a variety of other similar applications.

Acknowledgements

The authors would like to express their gratitude to Nanyang Technological University for the allocation of research fund and Singapore National Eye Centre for the supply of image data.

References

[1] T. McInerney, D. Terzopoulos, Deformable models in medical image analysis: a survey, Med. Image Anal. 1 (2) (1996) 91–108.
[2] M. Kass, A. Witkin, D. Terzopoulos, Snakes: active contour models, Int. J. Comput. Vision 1 (4) (1987) 321–331.
[3] T.F. Cootes, C.J. Taylor, D.H. Cooper, J. Graham, Active shape models—their training and application, Comput. Vision Image Understanding 61 (1) (1995) 38–59.
[4] S. Tamura, Y. Okamoto, K. Yanashima, Zero-crossing interval correction in tracking eye-fundus blood vessels, Pattern Recognition 21 (3) (1988) 227–233.
[5] Z. Liu, O. Chutatape, S.M. Krishnan, Automatic image analysis of fundus photography, Proc. IEEE-EMBS Chicago, USA, 2 (1997) 524–525.
[6] D.P. Huttenlocher, G.A. Klanderman, W.J. Rucklidge, Comparing images using the Hausdorff distance, IEEE Trans. Pattern Anal. Mach. Intell. 15 (9) (1993) 850–863.
[7] M. Lalonde, M. Beaulieu, L. Gagnon, Fast and robust optic disc detection using pyramidal decomposition and Hausdorff-based template matching, IEEE Trans. Med. Imag. 20 (11) (2001) 1193–1200.
[8] D.T. Morris, C. Donnison, Identifying the neuroretinal rim boundary using dynamic contours, Image Vision Comput. 17 (1999) 169–174.
[9] S. Lee, L. M. Brady, Integrating stereo and photometric stereo to monitor the development of glaucoma, Proceeding of the BMVC, Oxford, UK, 1990, pp. 193–198.
[10] M. Turk, A. Pentland, Eigenfaces for recognition, J. Cognitive Neurosci. 3 (1) (1991) 70–86.
[11] H. Li, O. Chutatape, Automatic location of optic disk in retinal images, Proceeding of the ICIP, Thessaloniki, Greece, 2001, pp. 837–840.
[12] D.R. Hill, A vector clustering technique, Mechanized Information Storage, Retrieval and Dissemination, North-Holland, Amsterdam, 1968.
[13] V. Chalana, Y. Kim, A methodology for evaluation of boundary detection algorithms on medical images, IEEE Trans. Med. Imag. 16 (5) (1997) 642–652.
[14] V. Chalana, D.T. Linker, D.R. Haynor, Y. Kim, A multiple active contour model for cardiac boundary detection on echocardiographic sequences, IEEE Trans. Med. Imaging 15 (3) (1996) 290–298.

About the Author—HUIQI LI received her B.E. and M.E. degrees from Harbin Institute of Technology, China in 1993 and 1995, respectively, and received her Ph.D. degree from Nanyang Technological University, Singapore in 2003, all in Electrical and Electronic Engineering. She was an electronic engineer with the Beijing Institute of Control Device, China from 1995 to 1999. Currently, she is a research fellow in the School of Computing, National University of Singapore. Her research interests include medical image processing, pattern recoginition, and computer vision.

About the Author—OPAS CHUTATAPE received the Ph.D. (1977) from Queen's University, in Electrical Engineering. His primary area of study was in communication and signal processing. He started his career after graduation as an operational engineer in the Telephone Organisation of Thailand, and later joined the academic line as a university lecturer. Eventually he was with the School of Electrical and Electronic Engineering (EEE) at Nanyang Technological University, Singapore, where he has been working there since the end of 1982 and presently as an associate professor. His main interest now is in multimedia communication, knowledge-based image processing, and pattern recognition. During his academic leave in 1994 he was attached to Imaging Technology, Bedford, USA, where he had made a contribution on the implementation of blood sample detection algorithm on a dedicated DSP-based image processing system. For over 20 years of teaching and supervising a number of research projects at various levels, he has made various contributions both in practical and theoretical aspects in his areas of interest.